


Extensive numerical simulations of surface growth with temporally correlated noise

Tianshu Song^{1,2} and Hui Xia^{1,*}

¹*School of Materials Science and Physics, China University of Mining and Technology, Xuzhou 221116, China*

²*School of Information and Control Engineering, China University of Mining and Technology, Xuzhou 221116, China*

 (Received 21 August 2020; revised 22 December 2020; accepted 23 December 2020; published 19 January 2021)

Surface growth processes can be significantly affected by long-range temporal correlations. In this work, we perform extensive numerical simulations of a (1+1)- and (2+1)-dimensional ballistic deposition (BD) model driven by temporally correlated noise, which is regarded as the temporal correlated Kardar-Parisi-Zhang universality class. Our results are compared with the existing theoretical predictions and numerical simulations. When the temporal correlation exponent is above a certain threshold, BD surfaces develop gradually faceted patterns. We find that the temporal correlated BD system displays nontrivial dynamic properties, and the characteristic roughness exponents satisfy $\alpha \simeq \alpha_{\text{loc}} < \alpha_s$ in (1+1) dimensions, which is beyond the existing dynamic scaling classifications.

DOI: [10.1103/PhysRevE.103.012121](https://doi.org/10.1103/PhysRevE.103.012121)

I. INTRODUCTION

Nonequilibrium growth processes described by the Kardar-Parisi-Zhang (KPZ) universality class have attracted the attention of researchers for several decades [1–3]. The KPZ equation, which was originally proposed to describe stochastic surface and interface growth and has been observed in many physical fields, reads [1]

$$\frac{\partial h(\mathbf{r}, t)}{\partial t} = \nu \nabla^2 h + \frac{\lambda}{2} (\nabla h)^2 + \eta(\mathbf{r}, t), \quad (1)$$

where $h(\mathbf{r}, t)$ is the height of the surface at position \mathbf{r} and time t , ν is the surface tension, λ represents the lateral dependence of growth velocity, and the stochastic force $\eta(\mathbf{r}, t)$ is usually Gaussian and uncorrelated in space and time.

One of the most important tasks to solve the KPZ equation is to obtain scaling exponents with different types of fluctuation in $(d + 1)$ dimensions. Scaling behavior is often characterized by the fluctuation of the growth height around its mean height. The characteristic quantity commonly used to investigate is interface width that follows a dynamic scaling form [4]:

$$W(L, t) = \left\langle \sqrt{\sum_{\mathbf{r}} [h(\mathbf{r}, t) - \bar{h}(t)]^2 / L} \right\rangle^{1/2} \sim L^\alpha f(t/L^z), \quad (2)$$

where the overbar denotes the spatial average in the \mathbf{r} direction with system size L , $\langle \dots \rangle$ stands for the average over different noise realizations. The scaling function $f(u) \sim u^\beta$ for $u \ll 1$ and $f(u) \rightarrow \text{const}$ for $u \gg 1$, and α , z , $\beta = \alpha/z$ are roughness, dynamic, and growth exponents, respectively. The KPZ equation with the Gaussian white noise has been well investigated. It is obtained exactly in the (1+1)-dimensional case, and gives $\alpha = 1/2$, $\beta = 1/3$, and $z = 3/2$. However, it

is very hard to solve exactly the KPZ equation in two cases: (i) the substrate dimension $d > 1$, and (ii) in the presence of the long-range correlated noise. In the latter case, the spatial correlations in KPZ system have been extensively investigated numerically and theoretically [5–14], while only a few studies discussed the KPZ equation with long-range temporal correlations [15–19].

It should be noted that analytical results on temporal correlations in surface growth are noticeably different based on several theoretical schemes, such as dynamic renormalization group (DRG) [20], Flory-like scaling approach (SA) [21], and self-consistent expansion (SCE) [16]. Recently, many effects on the temporal correlated KPZ system have been investigated numerically, and abundant results have been obtained correspondingly [17,18]. However, the inconsistencies still exist between the numerical simulations and theoretical predictions. Furthermore, the results in $d > 1$ are still rare when long-range temporal correlations are considered. Thus these issues motivate us to further investigate the KPZ universality class involving temporal correlations. In this article, we first revisit the ballistic deposition (BD) model with temporally correlated noise [22], which was thought to belong to the same universality class as the temporal correlated KPZ system. We adopt the hybrid simulations based on graphics processing units (GPUs) and CPUs to improve the computing efficiency by dozens of times [23–26], so that we can perform extensive numerical simulations for larger system sizes and longer grow times and more independent runs than the previous studies. For the (1+1)-dimensional case, we reinvestigate the numerical results, and compare with that of the previous studies [18,22], and obtain some nontrivial dynamic properties. Furthermore, we investigate the (2+1)-dimensional BD model in the presence of temporal correlations. Then we make a comparison with theoretical predictions.

The rest of this paper is arranged as follows. First, we introduce the method to generate desired long temporal correlated noise. Then we briefly describe the BD model with long-range

*Corresponding author: hxia@cumt.edu.cn

temporal correlations in (1+1) and (2+1) dimensions. After that, we exhibit our simulated results and present a discussion. Finally, a brief conclusion is given.

II. MODELS AND METHODS

A. Long-range temporal correlated noise

To investigate how temporally correlated noise affects scaling behavior of the BD model, it needs to generate a correlated sequence first. The desired correlation function has the following form:

$$C(\tau) = \langle \eta_t \eta_{t+\tau} \rangle \sim \tau^{2\theta-1}, \quad (5)$$

where θ is the temporal correlation exponent. Here we adopt the fast fractional Gaussian noise (FFGN) method that was proposed by Mandelbrot [27]. First, by introducing $u_n = aB^{-n}$ with $B = 2$, $a = 6$, and $r_n = e^{-u_n}$, the weight function is given by

$$W_n^2 = \frac{12(1-r_n^2)(B^{1/2-\theta} - B^{\theta-1/2})(aB^{-n})^{1-2\theta}}{\Gamma(2-2\theta)}, \quad (6)$$

and then two auxiliary functions are defined to be

$$\begin{aligned} X_1(u) &= [\zeta_1(u) - 0.5]/\sqrt{1-r^2}, \quad \text{for } t = 1, \\ X_t(u) &= rX_{t-1}(u) + [\zeta_t(u) - 0.5], \quad \text{for } t > 1, \end{aligned} \quad (7)$$

where $\zeta(u)$ is uncorrelated uniformly distributed noise in the interval $[-0.5, 0.5]$. Finally, we can obtain the desired correlation noise $\eta_t = \sum_{n=1}^N W_n X_t(u_n)$, where N is chosen in the value range of $[20, 45]$ in order to satisfy the noise correlation function (5) for different values of θ .

B. BD model in (1+1) dimensions

The BD model was initially introduced for explaining colloidal aggregates, and widely studied in the area of surface growth as the paradigmatic discrete model of the KPZ universality class [2]. The BD model has an even simpler growth version, namely, the nearest neighbor sticking rule, which has the following form in (1+1) dimensions:

$$h(x, t) = \max\{h(x, t) + \eta'(x, t), h(x-1, t), h(x+1, t)\}, \quad (8)$$

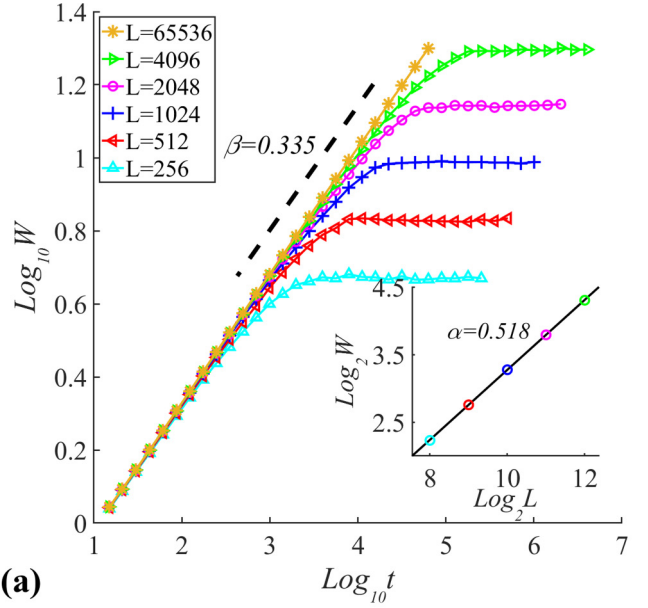
where $\eta'(x, t)$ is the binarized noise as the discrete version of the temporal correlated $\eta(x, t)$. More specifically, it is defined as $\eta'(x, t) = 1$ for $\eta(x, t) \geq 0$ and $\eta'(x, t) = 0$ for $\eta(x, t) < 0$.

C. BD model in (2+1) dimensions

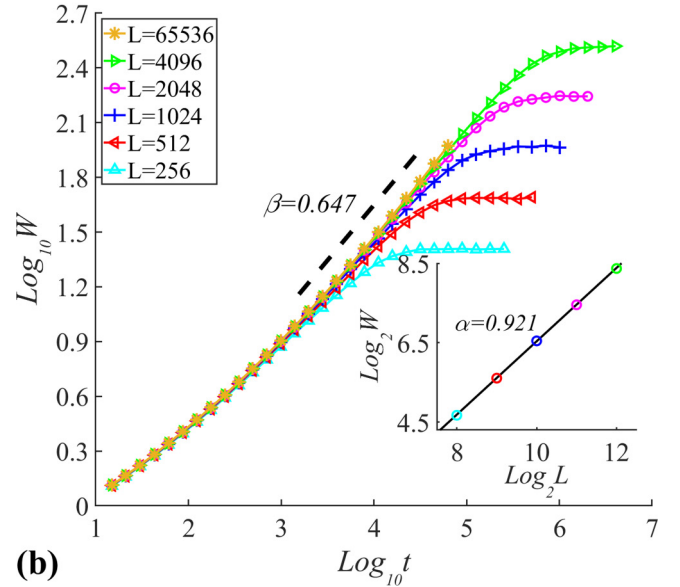
The BD model in (2+1) dimensions can be described as follows:

$$\begin{aligned} h(x, y, t+1) &= \max\{h(x, y, t) + \eta'(x, y, t), h(x-1, y, t), \\ &h(x+1, y, t), h(x, y-1, t), h(x, y+1, t)\}. \end{aligned} \quad (9)$$

Equation (9) indicates that a falling particle will stick to the highest particle of the four nearest neighbor positions around it. As an attempt, we also extend the BD grow rule for a falling particle sticking to the surrounding eight sites, i.e.,



(a)



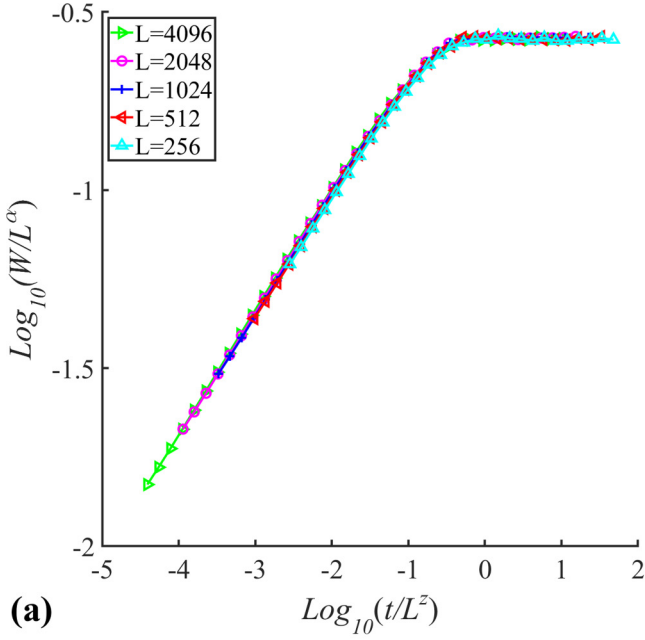
(b)

FIG. 1. The interface width $W(L, t)$ at different growth regimes with (a) $\theta = 0.05$; (b) $\theta = 0.45$. Results have been averaged over 1500 noise realizations, and these dotted lines are plotted to guide the eyes. The insets are the log-log plot of saturated interface width W_{sat} and system size L , and the solid lines are the fitting results with the values of global roughness exponent α .

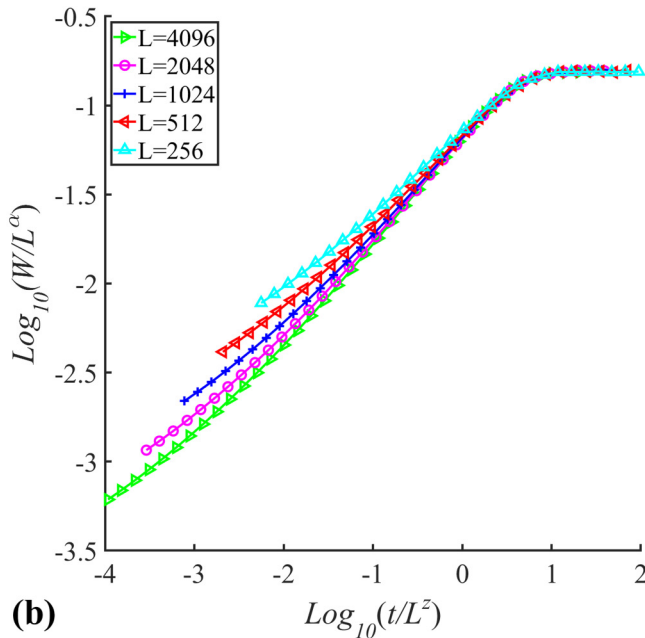
four nearest neighbors and four next-nearest neighbors, which reads

$$\begin{aligned} h(x, y, t+1) &= \max\{h(x, y, t) + \eta'(x, y, t), h(x-1, y, t), \\ &h(x+1, y, t), h(x, y-1, t), h(x, y+1, t), \\ &h(x-1, y-1, t), h(x+1, y+1, t), \\ &h(x+1, y-1, t), h(x-1, y+1, t)\}. \end{aligned} \quad (10)$$

Through performing simulations of both Eqs. (9) and (10), we find that adding next-nearest neighbor rule (10) does not affect the scaling properties in the (2+1)-dimensional BD model. In



(a)



(b)

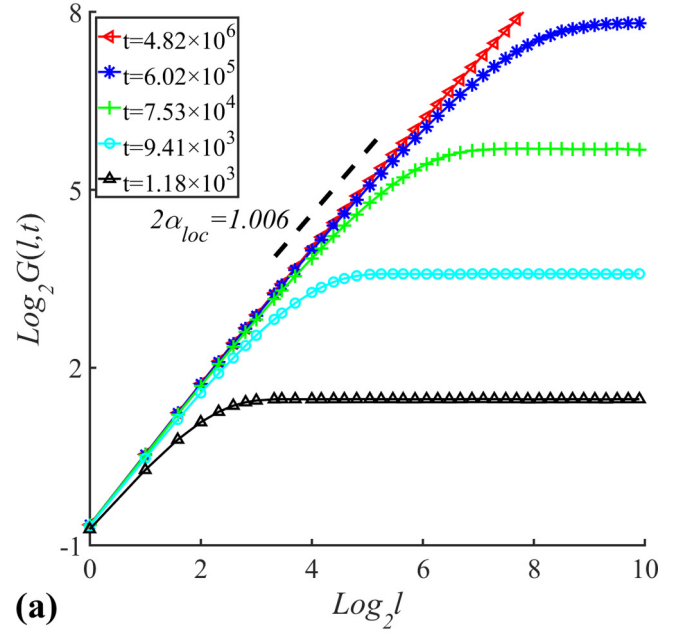
FIG. 2. The log-log plot of the scaled interface width vs the scaled growth time: (a) $\theta = 0.05$; (b) $\theta = 0.45$. Results show data collapses with the chosen critical exponents: (a) $\alpha = 0.52$ and $z = 1.55$; (b) $\alpha = 0.92$ and $z = 1.42$.

the following BD simulations, we will carry out our studies based on Eq. (9).

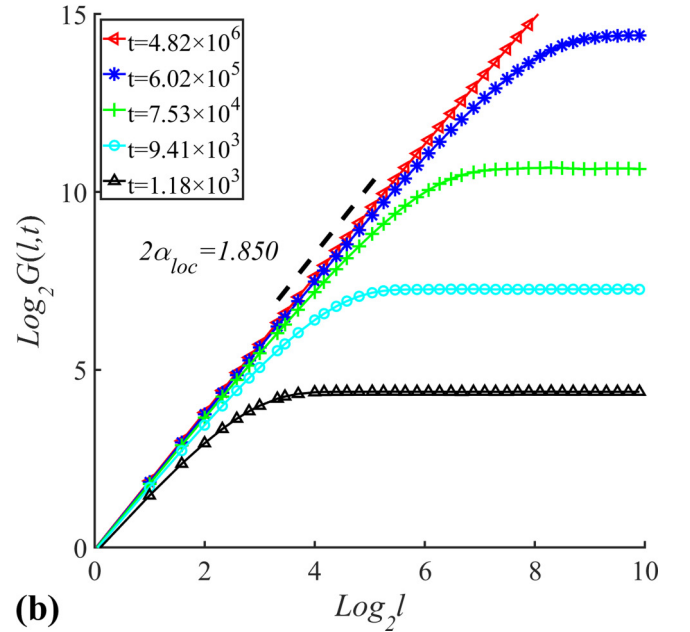
III. RESULTS AND DISCUSSIONS

A. BD model in (1+1) dimensions

We begin by analyzing the results of simulating the correlated BD model in (1+1) dimensions. At first, we calculate interface width $W(L, t)$ and then obtain the critical exponents based on power-law scaling from Eq. (2) in different growth regimes separated by a crossover growth time $t_{\times} \sim L^z$:



(a)



(b)

FIG. 3. The log-log plot of the height-height correlation function $G(l, t)$ vs l with $L = 4096$: (a) $\theta = 0.05$; (b) $\theta = 0.45$. Results have been averaged over 1500 noise realizations. For clear comparison, each curve shifts accordingly along the vertical coordinate.

$W(L, t) \sim t^\beta$ for $t \ll t_{\times}$ and $W(L, t) \sim L^\alpha$ for $t \gg t_{\times}$. Thus, in order to confirm BD scaling, we obtain the effective scaling exponents β and α in the early growth times and the saturated growth regimes, respectively. Considering large fluctuations of $W(L, t)$ with system size and growth time, we adopt the large system sizes and plenty of noise realizations in order to alleviate the fluctuations. In the following, numerical simulations of hybrid computing between GPUs and CPUs are performed extensively.

Figure 1 exhibits the log-log plot of the interface width $W(L, t)$ versus growth time t in the whole growth regimes

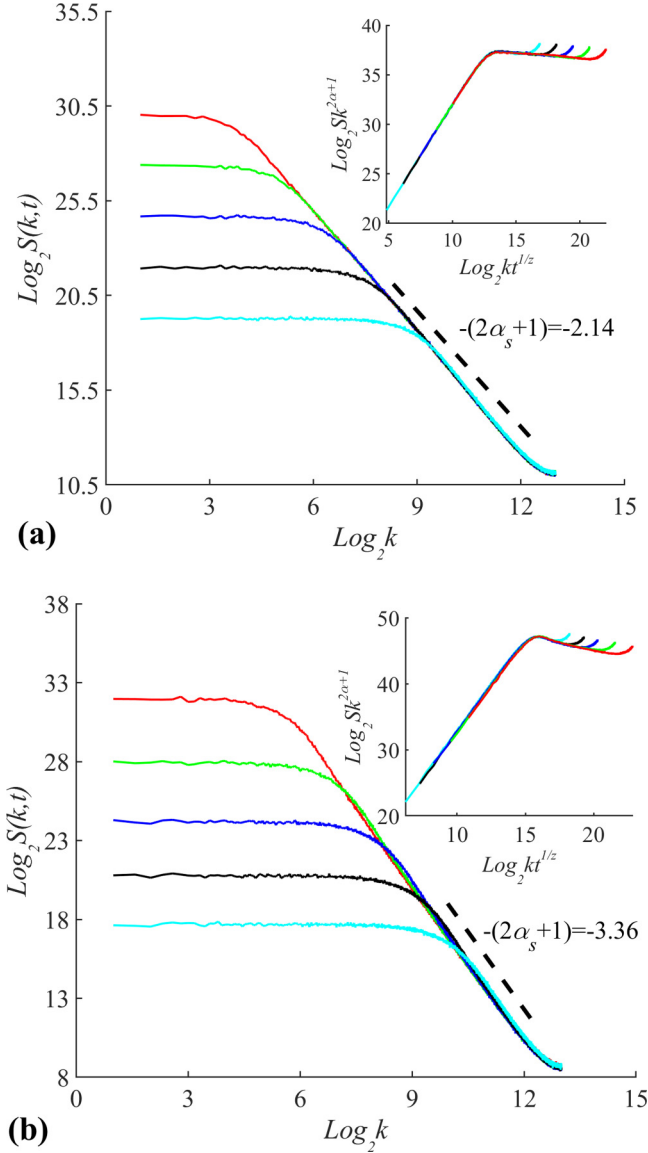


FIG. 4. The structure factor $S(k, t)$ of the growth interface at different growth times for the BD system in presence of the correlated noises: (a) $\theta = 0.05$; (b) $\theta = 0.45$. Results have been averaged over different noise realizations: 1500 for $\theta = 0.05$ and 500 for $\theta = 0.45$. Insets show good data collapses with the chosen critical exponents: (a) $\alpha = 0.518\text{--}0.538$ and $z = 1.55$; (b) $\alpha = 0.921\text{--}0.931$ and $z = 1.42$.

for the BD model with $\theta = 0.05$ and $\theta = 0.45$. In the early time regime $t \ll L^z$, we obtain the growth exponents $\beta = 0.335 \pm 0.013$ for $\theta = 0.05$, and $\beta = 0.647 \pm 0.007$ for $\theta = 0.45$. Here $L = 65\,536$ is used to increase the precision. To determine the values of α , system sizes are chosen in the range [256, 4096]. And in the saturated growth regime $t \gg L^z$, we obtain the global roughness exponents $\alpha = 0.518 \pm 0.006$ for $\theta = 0.05$, $\alpha = 0.921 \pm 0.013$ for $\theta = 0.45$ from the double-log plot of the saturated interface width as a function of the system size, as shown in the insets of Figs. 1(a) and 1(b), respectively.

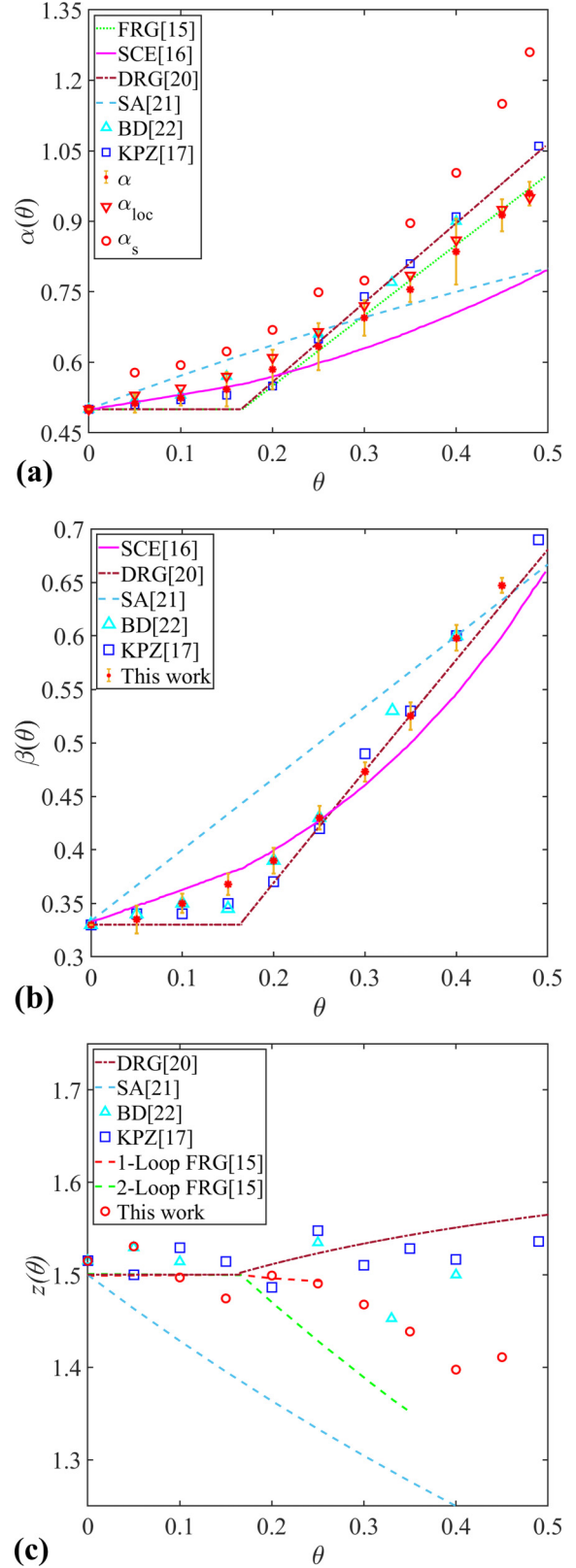


FIG. 5. The scaling exponents as a function of θ for the correlated BD model: (a) α vs θ ; (b) β vs θ ; (c) z vs θ . The existing theoretical predictions are also provided for comparison quantitatively.

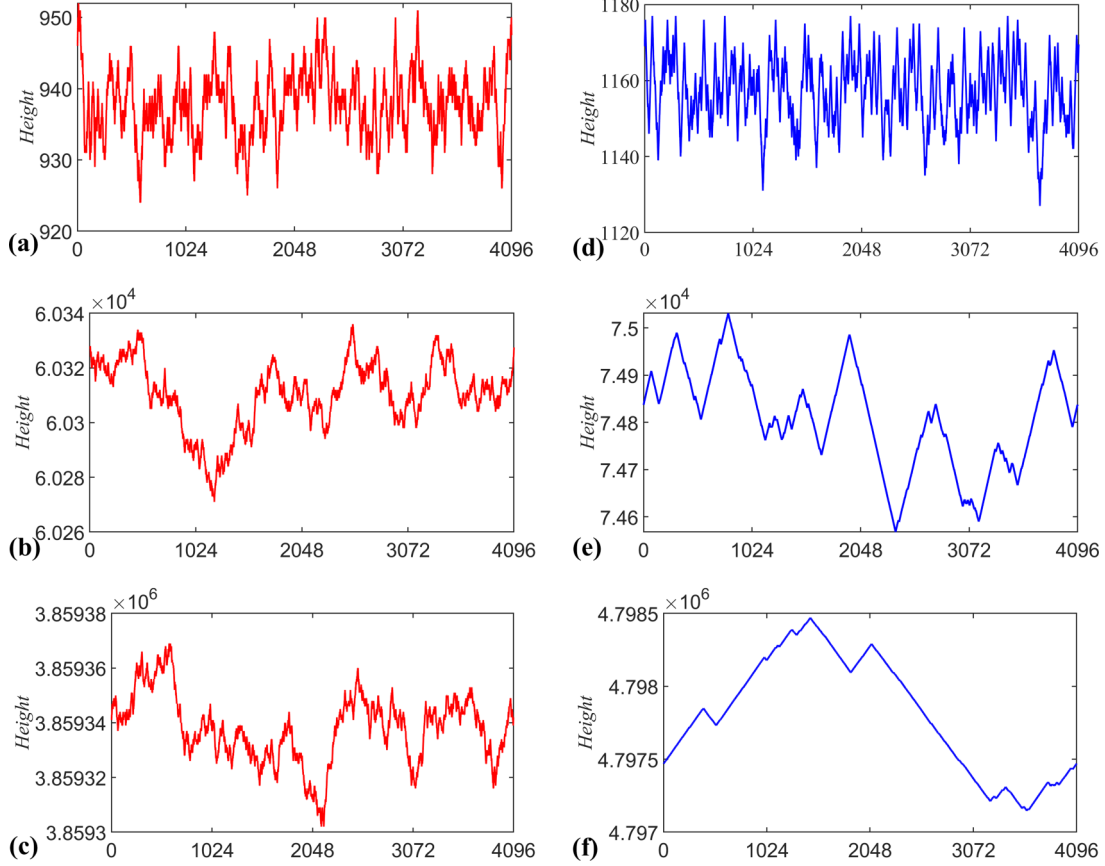


FIG. 6. The comparison of interface morphology in the (1+1)-dimensional correlated BD model with three growth regimes and two temporally correlated parameters: (a) $t = 1.2 \times 10^3$, (b) $t = 7.5 \times 10^4$, (c) $t = 4.8 \times 10^6$ for $\theta = 0.05$; and (d) $t = 1.2 \times 10^3$, (e) $t = 7.5 \times 10^4$, (f) $t = 4.8 \times 10^6$ for $\theta = 0.45$.

In order to make further numerical analysis of scaling exponents, we rescale the interface width by W/L^α which means vertical shifting of curves, and rescale growth time by t/L^z which means horizontal shifting. According to Eq. (2), these curves with different system sizes collapse into only one curve after rescaling, as shown in Fig. 2. These results also show that the dynamic exponents obtained independently from data collapses are consistent with the results obtained from the relation $z = \alpha/\beta$.

In addition to the scaling exponents of the interface width, the equal-time height difference correlation function $G(l, t)$ is also very important and informative. The function is defined as $G(l, t) = \langle (h(\mathbf{r} + \mathbf{l}, t) - h(\mathbf{r}, t))^2 \rangle$, where the brackets denote ensemble average. The local roughness exponent α_{loc} is determined from the relation $G(l, t) \sim l^{2\alpha_{\text{loc}}}$ ($l \ll L$). The relation $\alpha = \alpha_{\text{loc}}$ is always satisfied in a normal self-affine interface, and $\alpha \neq \alpha_{\text{loc}}$ indicates anomalous scaling in surface growth [28]. As for the BD model in (1+1) dimensions, we computed $G(l, t)$ with different θ , and obtained α_{loc} , as shown in Fig. 3. Here, we choose $t = 4.82 \times 10^6$, $l_1 = 8$, and $l_2 = 32$ in order to satisfy the local window sizes $l \ll L$. Our results show that $\alpha_{\text{loc}} \approx 0.503$ ($\theta = 0.05$) and $\alpha_{\text{loc}} \approx 0.925$ ($\theta = 0.45$). Compared with the global roughness exponents related to the interface width, we find that $\alpha_{\text{loc}} \approx \alpha$ from the whole θ regions. Therefore, in a certain sense, our results imply that normal self-affine scaling still

satisfies in the BD growth in presence of temporally correlated noise.

Furthermore, the structure factor $S(k, t) = \langle \hat{h}(k, t) \hat{h}(-k, t) \rangle$ also plays a vital role in revealing scaling properties of growth interface, where $h(k, t)$ is the Fourier transformation of $h(\mathbf{x}, t)$. For $(d+1)$ -dimensional growth surface, the structure factor satisfies the scaling form [29,30]

$$S(k, t) = k^{-(2\alpha+d)} s(kt^{1/z}),$$

with

$$s(u) \sim \begin{cases} u^{2(\alpha-\alpha_s)} u \gg 1 \\ u^{2\alpha+d} u \ll 1 \end{cases},$$

where $s(u)$ is a spectral scaling function and α_s is a spectral roughness exponent. The roughness process follows the normal Family-Vicsek (FV) scaling when $\alpha_s = \alpha$. On the contrary, anomalous scaling occurs when $\alpha \neq \alpha_s$. To determine the universal critical properties, we use a scaling function $S(k, t)k^{(2\alpha+d)}$ against $kt^{1/z}$. Furthermore, when $kt^{1/z} \gg 1$, $S(k, t)k^{(2\alpha+d)} \sim k^{-2(\alpha_s-\alpha)} t^{2(\alpha-\alpha_s)/z}$, and when $kt^{1/z} \ll 1$, $S(k, t)k^{(2\alpha+d)} \sim k^{(2\alpha+d)} t^{(2\alpha+d)/z}$. When the roughness and dynamic exponents are chosen effectively, all the data collapses into a single universal curve for different wave number regimes. Therefore, we can estimate the critical exponents α and z based on data collapse. Meanwhile, we also check

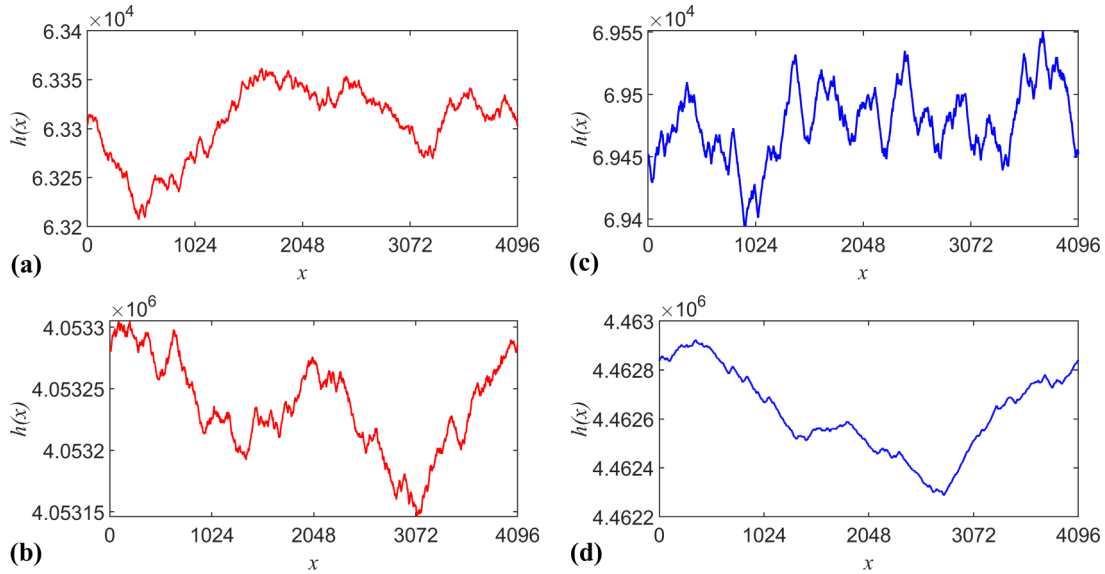


FIG. 7. The comparison of interface morphology in (1+1)-dimensional correlated BD model with three growth regimes and two temporally correlated parameters: (a) $t = 7.5 \times 10^4$, (b) $t = 4.8 \times 10^6$ for $\theta = 0.20$; and (c) $t = 7.5 \times 10^4$, (d) $t = 4.8 \times 10^6$ for $\theta = 0.35$.

the dynamical exponent obtained independently based on the scaling relation $z = \alpha/\beta$.

Figure 4 shows the double logarithmic plot of the structure factor $S(k, t)$ versus wave number k with various temporal correlation parameters. Compared with different sizes and growth times, we find that the scaling properties of the structure factor do not change evidently with L and t . Figure 4(a) shows the log-log plot of $S(k, t)$ versus k with $\theta = 0.05$. Figure 4(b) provides the numerical results with $\theta = 0.45$. Using the scaling relation $S(k, t) \sim k^{-(2\alpha_s + d)}$ in the large wave number regime, one can obtain the spectral roughness exponent α_s as an independent exponent. When $\theta = 0.05$, we obtain $\alpha_s = 0.57 \pm 0.01$. Based on data collapses, we obtain independently $\alpha = 0.52$ and $z = 1.55$, as shown in Fig. 4(a). We find that the global roughness exponents are evidently less than the corresponding spectral scaling exponents obtained directly through $S(k, t)$ against k . Thus our results provide numerical evidences that nontrivial scaling can occur even in the small θ region. In Fig. 4(b), we choose $\theta = 0.45$ as a typical example of the correlated BD system for the large θ region, and obtain $\alpha_s = 1.18 \pm 0.02$. Here, the critical exponents used for data collapse are $\alpha = 0.92$ and $z = 1.42$, which is consistent with the values obtained from Eq. (2). Remarkably, we find that the spectral roughness exponent is not equal to either local or global roughness exponents, and the latter two roughness exponents are nearly equal to each other. Therefore, these results imply that the BD system within the large θ region displays nontrivial dynamical scaling. It is

quite remarkable that $\alpha \approx \alpha_{loc} \neq \alpha_s$ does not satisfy dynamic scaling classifications [31].

In order to effectively reduce the finite-size effects, our results are obtained for the system of larger size. We estimate quantitatively α , α_{loc} , and α_s in the stable scaling regions with different θ . We find that the value α_s is always larger than the local and global roughness exponents in presence of long-range correlations, which slightly differs from the recent numerical results [18]. For the sake of comparison, Fig. 5 also includes the previous theoretical predictions and numerical simulations of KPZ and BD system driven by temporally correlated noise. For the global roughness exponents, with comparison of the previous theoretical predictions, we find that our results are consistent with SCE predictions in the small θ region, and are in agreement with FRG in the large θ region. Furthermore, we also find that $\alpha \approx \alpha_{loc}$ in the whole correlation region, which implies that the interface of the BD model with long-range temporally correlated noise still displays a self-affine fractal from a certain sense. And the dynamic exponents can be obtained using $z = \alpha/\beta$, and meanwhile, we also obtain it based on good data collapses from the scaled interface width and structure factor. It should be noted that these values obtained independently are consistent with each other.

Next, we provide an intuitive evidence of the morphology evolution with different growth times and temporal correlations. Figure 6 clearly shows that the interface profiles of the BD model can be obviously affected by long-range temporally

TABLE I. Roughness exponents of the KPZ universality class in (2+1) dimensions.

Model	HSM [32]	BCSOS [33]	RSOS [34–37]	DPRM [38]	BD [39]	KPZ [38,40]	DLC [25,41]	Our results
α	0.385	0.38	0.38–0.393	0.385	0.363–0.366	0.38–0.4	0.377–0.393	0.390

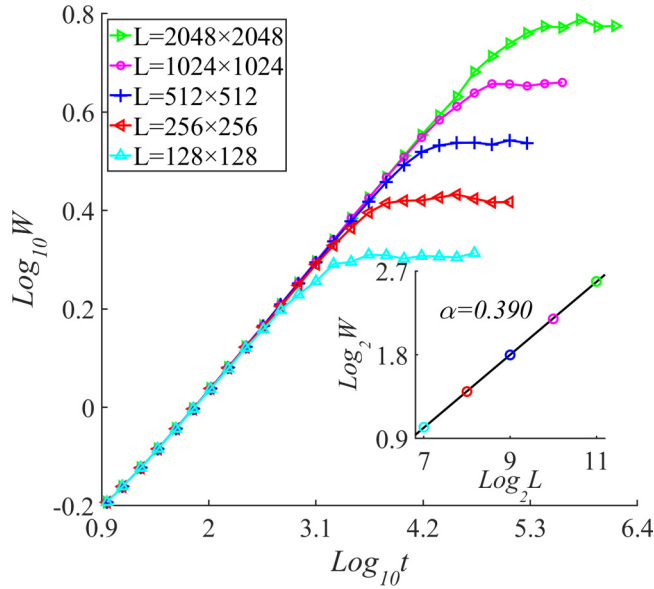
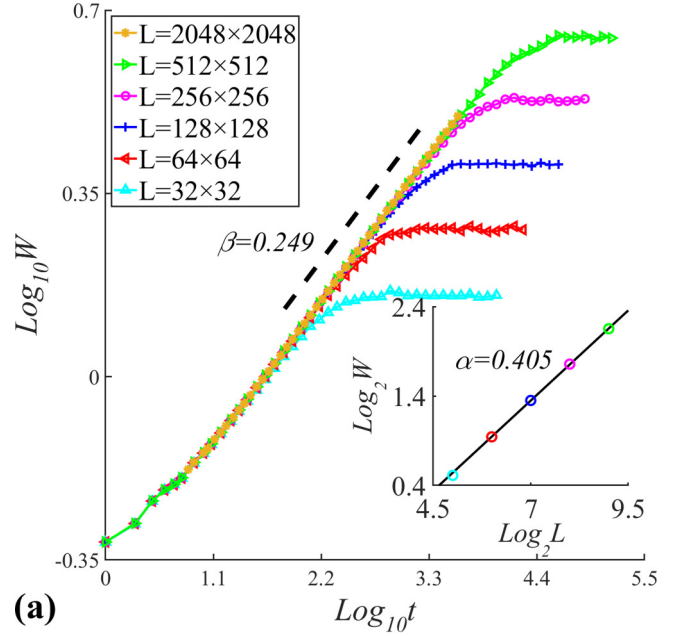


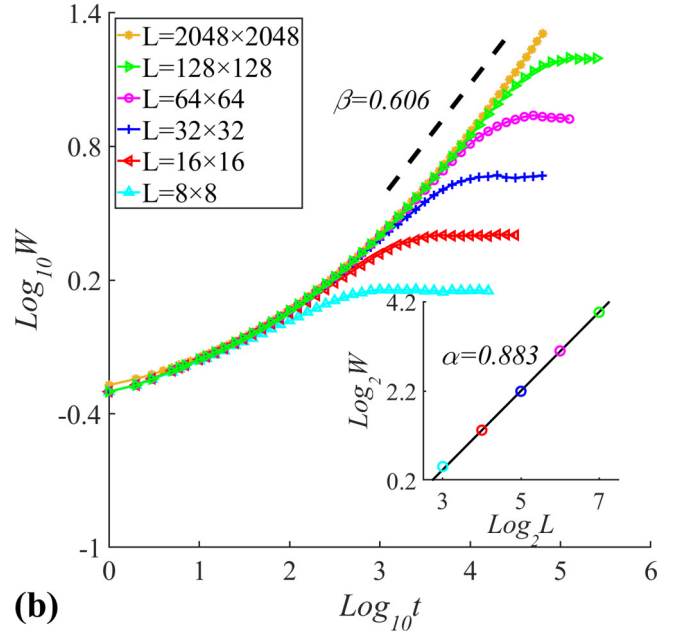
FIG. 8. $W(L, t)$ vs t in (2+1)-dimensional BD without temporal correlation. Inset exhibits W_{sat} against L .

correlated noise. Figures 6(a)–6(c) exhibit the typical profiles of growth interface in early, intermediate, saturated growth regimes for $\theta = 0.05$. We can easily observe that, from the early growth to the saturation regions, the BD model with small temporal correlations exhibits a self-affine interface, which differs drastically from the case of large temporal correlations. This observation is consistent with the consequence that the self-affine fractal still appears for the small temporal correlations. However, when noise correlation exponent θ increases gradually, the self-affine fractal will be destroyed, and the interface develops faceted patterns that completely dominate the dynamics in the saturated growth region. The evident change will happen when the temporal correlation exponent is beyond the critical threshold [18]. Figures 6(d)–6(f) exhibit the morphology of surface height with different growth regimes for $\theta = 0.45$. We find that, when increasing temporal correlations and reaching the long growth time limit, the similar interfaces at small and large scales are gradually formed, and thus the local and global roughness satisfies statistical similarity, which evidently differs from anomalous roughening where $\alpha \neq \alpha_{\text{loc}}$ [31]. We also find that, when θ is close to 0.5, the values of both α and α_{loc} approach 1 in the (1+1)-dimensional case.

In order to explore qualitatively the crossover effects from the self-affine to the mounded pattern, we display the surface morphology with $\theta = 0.20$ and 0.35 , as shown in Fig. 7. Interestingly, we find that there exists a critical threshold θ_c between the two values of θ . When $\theta = 0.20$, both the early and saturated surfaces all display self-affine, and there are no obvious mounds. However, one can find the mounds in the saturated growth regime with $\theta = 0.35$. The differences of surface morphology imply that there exists a nontrivial scaling transient from small to large θ in the temporal correlated BD model, which is closely related to anomalous scaling in the KPZ subject to temporally correlated noise [18].



(a)



(b)

FIG. 9. The log-log plot of surface width vs growth time in (2+1) dimensions: (a) $\theta = 0.05$; (b) $\theta = 0.45$. Results have been averaged over 500 noise realizations, and these dotted lines are plotted to guide the eyes. The insets are the log-log plot of saturated surface width W_{sat} and system size L , and the solid lines are the fitting results with the values of global roughness exponent α .

B. BD model in (2+1) dimensions

As far as we know, numerical and theoretical investigation on surface growth with long-range temporal correlation in (2+1) dimensions is very rare. As a special case of temporal correlation, namely, $\theta = 0$, we first revisit BD simulations without temporal correlated noise. In these simulations, FFGN is not used, and most GPU memory and computing resources are reserved, thus larger system sizes have been applied to perform numerical simulations. The

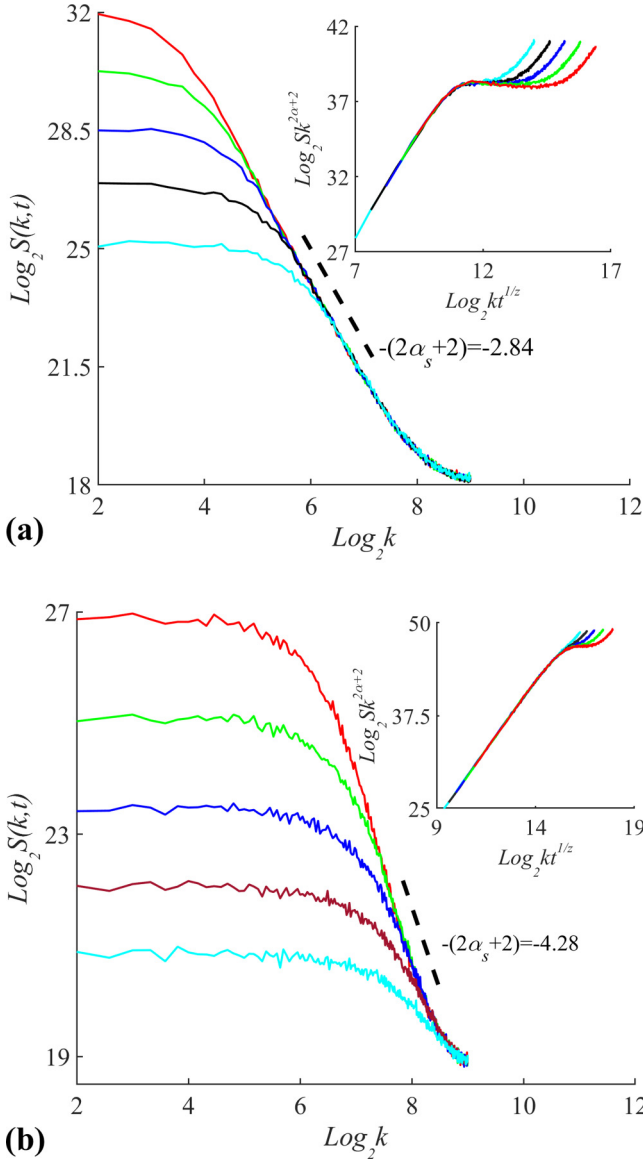


FIG. 10. The structure factor $S(k, t)$ of the growth surface at different growth times for (2+1)-dimensional BD system in presence of the correlated noises: (a) $\theta = 0.05$; (b) $\theta = 0.45$. Insets show good data collapses with the chosen critical exponents: (a) $\alpha = 0.415 \pm 0.010$ and $z \approx 1.60$; (b) $\alpha = 0.870 \pm 0.010$ and $z \approx 1.40$. The system size $L = 1024 \times 1024$ is used, and data are averaged over 500 independent noise realizations.

numerical results of the BD model without temporally correlated noise are shown in Fig. 8.

Without temporal correlation, the main numerical results of (2+1)-dimensional KPZ universality class are listed in Table I. We find that most recent results show $0.38 < \alpha < 0.40$, and we obtain $\alpha \approx 0.390$ when $\theta = 0$, which is also consistent with previous studies.

When $\theta \neq 0$, from the perspective of analytic approximations, it is difficult to analyze theoretically the (2+1)-dimensional KPZ system. For numerical simulation, one immediate limitation is that when performing simulations of long-range correlations in (2+1) dimensions, it will take too much time to obtain reasonable results as system size in-

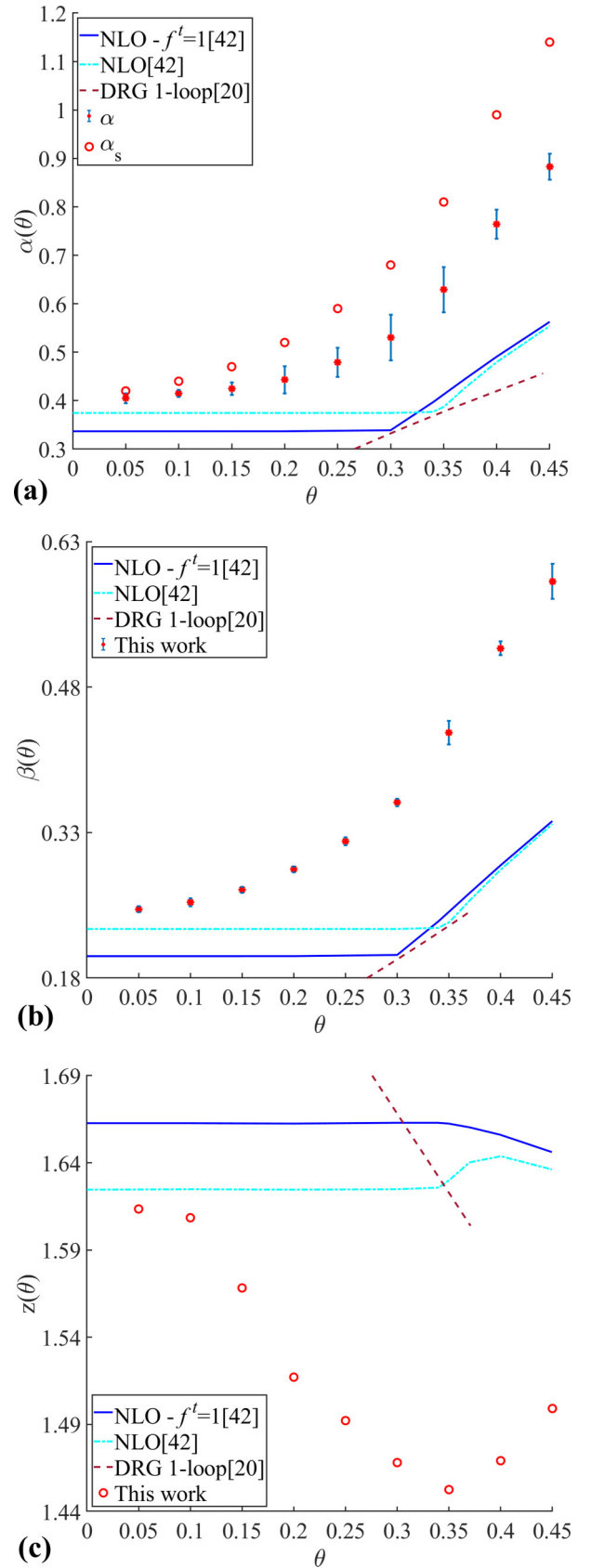


FIG. 11. The values of critical exponents in (2+1) dimensions: (a) α and α_s ; (b) β , (c) z .

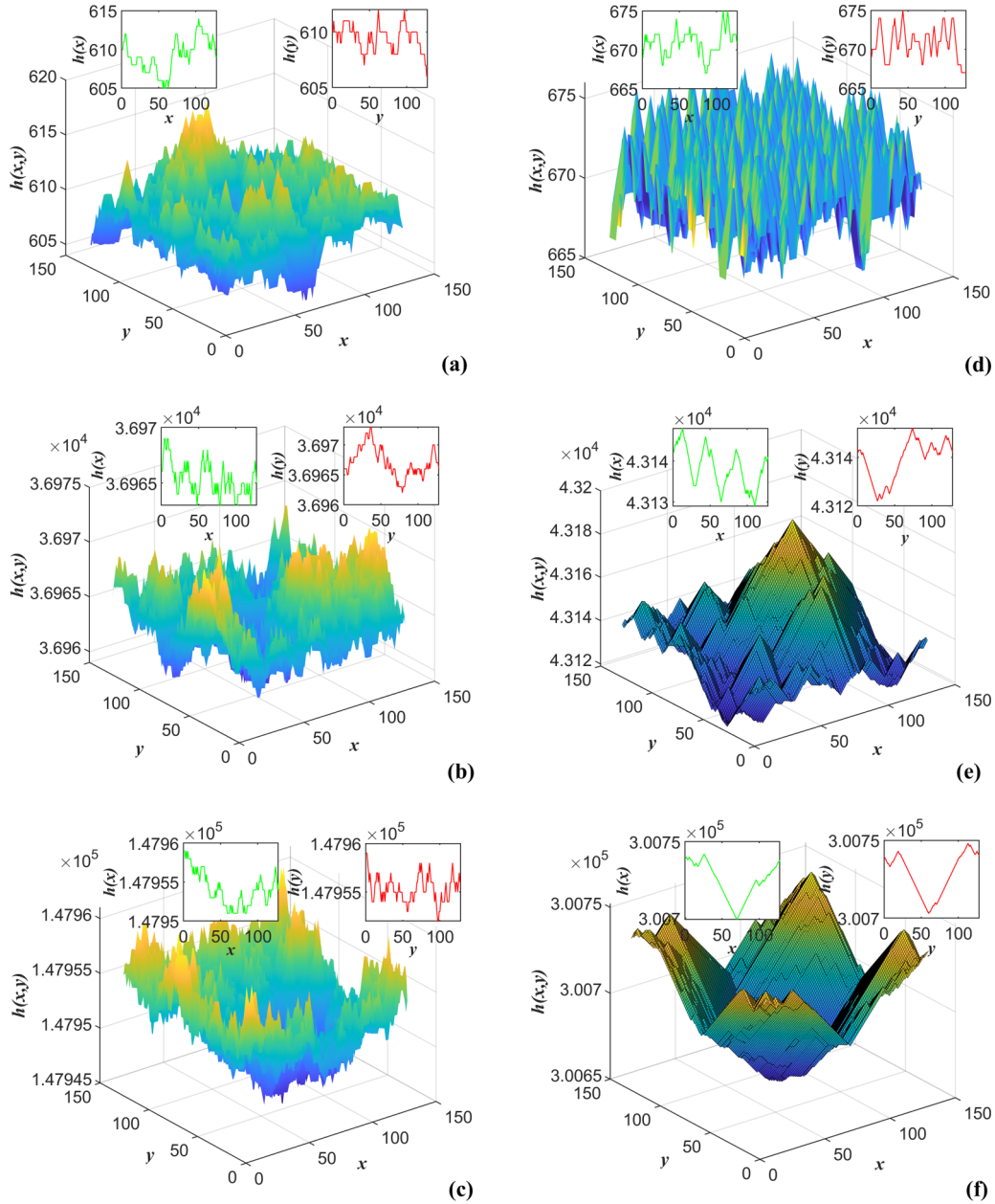


FIG. 12. The surface morphology in (2+1)-dimensional BD model with $\theta = 0.05$ at different growth times: (a) $t = 6.75 \times 10^2$; (b) $t = 4.32 \times 10^4$; (c) $t = 1.73 \times 10^5$; and with $\theta = 0.45$ at different growth times: (d) $t = 6.75 \times 10^2$; (e) $t = 4.32 \times 10^4$; (f) $t = 3.01 \times 10^5$. The subgraphs of each subfigure are height of cross section at $X = 1$ (L) and $Y = 1$ (R).

creases. In our simulations, the system size 2048×2048 is used to obtain growth exponent, and the largest size 512×512 is used for roughness exponent calculations. It should be noted that both (9) and (10) of the BD model have consistent results. The scaling behavior and the obtained critical exponents based on computing the global surface width for $\theta = 0.05$ and $\theta = 0.45$ are illustrated in Fig. 9. For $\theta = 0.05$, we obtain $\beta = 0.249 \pm 0.003$ and $\alpha = 0.405 \pm 0.010$, and for $\theta = 0.45$, $\beta = 0.606 \pm 0.005$ and $\alpha = 0.883 \pm 0.015$. Therefore, temporal correlations can affect evidently the scaling behavior at both the early growth and saturated regions for the (2+1)-dimensional case.

In order to further investigate scaling behavior in (2+1) dimensions, we also calculate the structure factors, which are

summarized to show in Fig. 10. We obtained $\alpha_s = 0.42 \pm 0.02$ for $\theta = 0.05$ and $\alpha_s = 1.14 \pm 0.03$ for $\theta = 0.45$. It is easy to find that the difference between global and spectrum roughness exponents is more evident as θ increases.

Figure 11 shows our numerical values of the (2+1)-dimensional BD system driven by temporally correlated noise, and the main theoretical predictions are given for comparison correspondingly. The results of α and α_s against θ are shown in Fig. 11(a), and the growth exponents with temporal correlations are listed in Fig. 11(b). Obviously, our results are consistent with the previous numerical results when θ approaches 0. Through the comparison, our results are not close to the theoretical predictions of the one-loop DRG technique [20] and the nonperturbative renormalization group

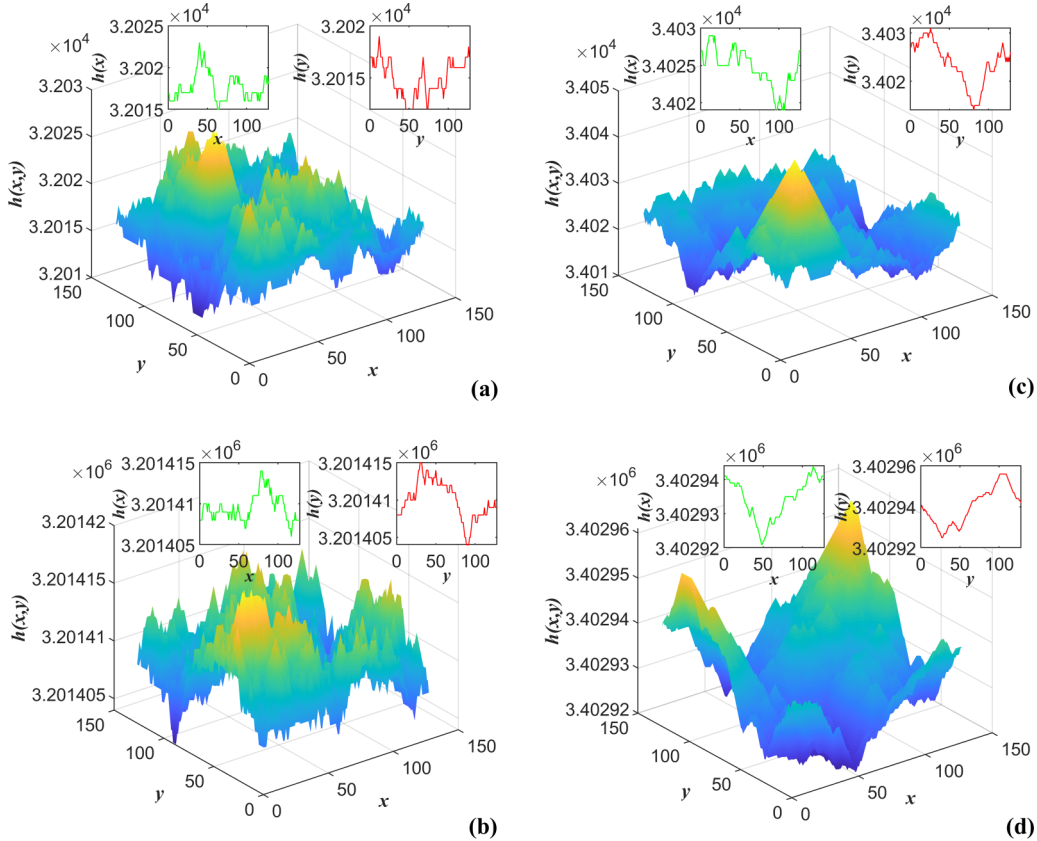


FIG. 13. The crossover from self-affine to mounded pattern in simulating BD model from small to large temporal correlations with different growth times: (a) $t = 3.529 \times 10^4$, (b) $t = 3.529 \times 10^6$ ($\theta = 0.20$); (c) $t = 3.529 \times 10^4$, (d) $t = 3.529 \times 10^6$ ($\theta = 0.35$). The subgraphs of each subfigure are height of cross section at $X = 1$ (L) and $Y = 1$ (R).

(NPRG) approach [42], thus more theoretical and numerical methods are still required to make further investigations and comparisons. Our results show that the temporal correlated BD system in (2+1) dimensions displays nontrivial dynamical scaling. Remarkably, similar to (1+1) dimensions, we also observe that $\alpha < \alpha_s$ still satisfies for the large temporal correlation region in the most physically relevant dimension.

Figure 12 exhibits the surface morphology of the (2+1)-dimensional BD model driven by correlated noise located at different growth time regions. Similar to the (1+1)-dimensional case, for the small noise correlation exponent θ ($\theta = 0.05$), the growth surfaces appear as self-affine fractal structures at different growth regimes, as shown in Figs. 12(a)–12(c). However, for large correlation exponents θ ($\theta = 0.45$), one can see from Figs. 12(d)–12(f) that, as growth time increases, mound sizes can be clearly observed and many little mounds tend to merge into large mounds. We suppose that, when θ gradually approaches 0.5, the mounded surface of the BD model in (2+1) dimensions may eventually evolve into the shaped of one isolated faceted pattern in the long time limit.

In order to investigate the crossover effect for the self-affine to the mounded pattern in (2+1) dimensions, we display the surface morphology with different θ . We find that there exists a critical threshold θ_c between $\theta = 0.20$ and $\theta = 0.35$. Interestingly, we observe from Fig. 13 that when $\theta = 0.20$, the saturated surfaces display self-affine, and there are no obvious mounds. However, one can find the mounds in the

saturated growth regime with $\theta = 0.35$. The differences of surface morphology imply that there is a critical threshold θ_c for the appearance of mounded shaped surfaces in the BD model, and also closely related to anomalous scaling [18]. Therefore, (2+1) dimensions have similar properties to the (1+1)-dimensional case, and there exists the critical threshold in (1+1) dimensional cases, both linear Edwards-Wilkinson (EW) and nonlinear KPZ growth systems, in the presence of temporally correlated noise ($\theta_\tau \approx 1/4$) [18,43]. These results discussed above also imply that the critical threshold in the stochastic growth model driven by the temporally correlated noise is universal, which is independent on the substrate dimensions.

IV. CONCLUSION

In this work, we have studied numerically the BD model with temporal correlations in (1+1) and (2+1) dimensions. Our results show that, in the (1+1)-dimensional case, the critical exponents are consistent with SCE predictions in the small θ region, and are in agreement with FRG in the large θ region. We find that surface morphology is obviously changed with temporal correlations, however, α_{loc} equals α , which implies that the whole growth in the BD model subject to long-range temporally correlated noise still satisfies the self-affine fractal statistically. For the (2+1)-dimensional case, we have obtained the values of scaling exponents in the whole θ region. As a special case, when $\theta \rightarrow 0$, our results are consistent

with the existing numerical and theoretical predictions. When $\theta > 0$, we find that temporal correlations affect evidently the scaling behavior during the whole growth regions, and unfortunately, our results are not close to the existing theoretical predictions of both NLO and DRG approaches. It should be noted that, based on the existing dynamic scaling classifications [31], the scaling properties of surface growth are divided into four types by comparing the values of $\alpha, \alpha_{loc}, \alpha_s$, i.e., (i) $\alpha = \alpha_{loc} = \alpha_s$; (ii) $\alpha \neq \alpha_{loc} = \alpha_s$; (iii) $\alpha = \alpha_s, \alpha_{loc} = 1$; (iv) $\alpha \neq \alpha_s, \alpha_{loc} = 1$. However, our results exhibit nontrivial scaling behavior in the BD model with temporal correlations, more precisely, $\alpha \approx \alpha_{loc} < \alpha_s$ in (1+1) dimensions and $\alpha < \alpha_s$ in the (2+1)-dimensional case in the temporal correlated BD model.

As the typical model of the KPZ universality class, the BD model with Gaussian white noise exhibits normal scaling behavior. However, the BD model driven by the temporally correlated noise reveals nontrivial dynamic properties. Strong temporal correlations in both (1+1) and (2+1) dimensions

significantly change surface morphology and critical exponents. In the presence of the long-range temporal correlations, there are still differences between the BD and KPZ systems. For example, we do not need to binarize noise into 0 or 1 in the discretized KPZ equation. It remains unclear that how it affects the growth process when introducing the binarization of the correlated noise in the discrete models. So further investigation of the temporal correlated growth system is still necessary. Furthermore, we believe that our results can be of great interest for other problems involving the same universality class of the temporal correlated KPZ growth and other growth systems.

ACKNOWLEDGMENTS

We would like to thank W. Wang and Y. Wang for useful discussions and critical reading of the manuscript. This work was supported by the National Natural Science Foundation of China under Grant No. 51704293.

-
- [1] M. Kardar, G. Parisi, and Y.-C. Zhang, *Phys. Rev. Lett.* **56**, 889 (1986).
- [2] A.-L. Barabási and H. E. Stanley, *Fractal Concepts in Surface Growth* (Cambridge University Press, Cambridge, UK, 1995).
- [3] D. Squizzato, L. Canet, and A. Minguzzi, *Phys. Rev. B* **97**, 195453 (2018).
- [4] F. Family and T. Vicsek, *J. Phys. A* **18**, L75 (1985).
- [5] P. Meakin and R. Jullien, *Europhys. Lett.* **9**, 71 (1989).
- [6] P. Meakin and R. Jullien, *Phys. Rev. A* **41**, 983 (1990).
- [7] C.-K. Peng, S. Havlin, M. Schwartz, and H. E. Stanley, *Phys. Rev. A* **44**, R2239(R) (1991).
- [8] J. G. Amar, P.-M. Lam, and F. Family, *Phys. Rev. A* **43**, 4548 (1991).
- [9] E. Katzav and M. Schwartz, *Phys. Rev. E* **60**, 5677 (1999).
- [10] T. Halpin-Healy, *Phys. Rev. A* **42**, 711 (1990).
- [11] Y.-C. Zhang, *Phys. Rev. B* **42**, 4897 (1990).
- [12] E. Frey, U. C. Täuber, and H. K. Janssen, *Europhys. Lett.* **47**, 14 (1999).
- [13] A. Kr. Chattopadhyay and J. K. Bhattacharjee, *Europhys. Lett.* **42**, 119 (1998).
- [14] S. Chu and M. Kardar, *Phys. Rev. E* **94**, 010101(R) (2016).
- [15] A. A. Fedorenko, *Phys. Rev. B* **77**, 094203 (2008).
- [16] E. Katzav and M. Schwartz, *Phys. Rev. E* **70**, 011601 (2004).
- [17] T. Song and H. Xia, *J. Stat. Mech.* (2016) 113206.
- [18] A. Alés and J. M. López, *Phys. Rev. E* **99**, 062139 (2019).
- [19] P. Strack, *Phys. Rev. E* **91**, 032131 (2015).
- [20] E. Medina, T. Hwa, M. Kardar, and Y.-C. Zhang, *Phys. Rev. A* **39**, 3053 (1989).
- [21] Hanfei and B. Ma, *Phys. Rev. E* **47**, 3738 (1993).
- [22] C.-H. Lam, L. M. Sander, and D. E. Wolf, *Phys. Rev. A* **46**, R6128(R) (1992).
- [23] Y.-C. Zhang, *Physica A* **170**, 1 (1990).
- [24] H. Schulz, G. Ódor, G. Ódor, and M. F. Nagy, *Comput. Phys. Commun.* **182**, 1467 (2011).
- [25] J. Kelling and G. Ódor, *Phys. Rev. E* **84**, 061150 (2011).
- [26] G. Ódor, J. Kelling, and S. Gemming, *Phys. Rev. E* **89**, 032146 (2014).
- [27] B. B. Mandelbrot and J. R. Wallis, *Water Resour. Res.* **5**, 228 (1969).
- [28] G. Palasantzas and J. Krim, *Phys. Rev. B* **48**, 2873 (1993).
- [29] J. M. López, M. A. Rodríguez, and R. Cuerno, *Phys. Rev. E* **56**, 3993 (1997).
- [30] M. Siegert, *Phys. Rev. E* **53**, 3209 (1996).
- [31] J. J. Ramasco, J. M. López, and M. A. Rodríguez, *Phys. Rev. Lett.* **84**, 2199 (2000).
- [32] B. M. Forrest and L.-H. Tang, *Phys. Rev. Lett.* **64**, 1405 (1990).
- [33] C.-S. Chin and M. den Nijs, *Phys. Rev. E* **59**, 2633 (1999).
- [34] A. Pagnani and G. Parisi, *Phys. Rev. E* **92**, 010101(R) (2015).
- [35] J. Kondev, C. L. Henley, and D. G. Salinas, *Phys. Rev. E* **61**, 104 (2000).
- [36] E. Marinari, A. Pagnani, and G. Parisi, *J. Phys. A* **33**, 8181 (2000).
- [37] J. Kelling, G. Ódor, and S. Gemming, *Phys. Rev. E* **94**, 022107 (2016).
- [38] T. Halpin-Healy, *Phys. Rev. Lett.* **109**, 170602 (2012).
- [39] F. D. A. Aarao Reis, *Phys. Rev. E* **63**, 056116 (2001).
- [40] V. G. Miranda and F. D. A. Aarao Reis, *Phys. Rev. E* **77**, 031134 (2008).
- [41] G. Odor, B. Liedke, and K.-H. Heinig, *Phys. Rev. E* **79**, 021125 (2009).
- [42] D. Squizzato and L. Canet, *Phys. Rev. E* **100**, 062143 (2019).
- [43] A. Alés and J. M. López, *J. Stat. Mech.* (2020) 033210.